RESEARCH ARTICLE

ADVANCED
INTELLIGENT
SYSTEMS
Open Access

www.advintellsyst.com

Octopus-Inspired Suction Cups with Embedded Strain Sensors for Object Recognition

Ebrahim Shahabi,* Francesco Visentin, Alessio Mondini, and Barbara Mazzolai*

The octopus has unique capacities are sources of inspiration in developing soft robotic-enabling technologies. Herein, soft, sensorized, suction cups inspired by the suckers of *Octopus vulgaris* are presented. The suction cups using direct casting are fabricated, so that materials with different mechanical properties can be combined to optimize sensing and grasping capabilities. The artificial suckers integrate four embedded strain sensors, individually characterized and placed in a 90° configuration along the rim of the suction cup. Based on this arrangement, how well the sensory suction cup can detect 1) the direction and 2) the angle (from 30° to 90°) of a touched inclined surface and 3) the stiffness of a touched flat object (shore hardness between 0010 and D50) both in air and underwater is evaluated. Data processing on neural networks is based using a multilayer perceptron to perform regression on individual properties. The results show a mean absolute error of 0.98 for angles, 0.02 for directions, and 97.9% and 93.5% of accuracy for the material classification in air and underwater, respectively. In view of the results and scalability in manufacturing, the proposed artificial suckers would seem to be highly effective solutions for soft robotics, including blind exploration and object recognition.

1. Introduction

Octopuses have a fully boneless body and as well distributed intelligence, the ability to stretch, change the stiffness, and sense perception in all the body. This makes them the perfect source of inspiration for soft robotics technologies.[1] The abilities of

E. Shahabi
Scuola Superiore Sant'Anna, Biorobotics Institute
56025 Pontedera, PI, Italy
E-mail: ebrahim.shahabishalghouni@iit.it

E. Shahabi, F. Visentin, A. Mondini, B. Mazzolai
Bioinspired Soft Robotics Lab
Istituto Italiano di Tecnologia
16163 Genova, GE, Italy
E-mail: Barbara.mazzolai@iit.it

F. Visentin
Università degli Studi di Verona
37134 Verona, VR, Italy

The ORCID identification number(s) for the author(s) of this article can be found under https://doi.org/10.1002/aisy.202200201.

octopuses have been imitated in robotics to develop artificial suckers[2–4] and soft robotic arms.[5–8] Chemotactile sensing and the adhesion of suckers are used in combination with arm movements to explore environments, manipulate objects, and capture prey, as well as for anchoring and locomotion.[9–14]

An octopus can feel a slight touch in any part of its body since it is covered with mechanoreceptors, and the sense of touch is at its most sensitive in the suckers.[15] The sucker consists of two main regions connected by an orifice: the infundibulum, an exposed disk-like portion of the sucker, and the acetabulum, a spheroidal cavity with a protuberance at the base (**Figure 1**B). These regions have radial and meridional muscles (used for attachment) and circular muscles (used for active detachment).[14] Octopuses distinguish the shape and texture of objects using suckers with mechanoreceptors (Figure 1A).[16,17] Imitating these abilities in soft arms can lead to the development of a new generation of manipulators for blind exploration and manipulation in environments where there are no visual clues.

Bioinspiration from octopus' suckers can provide artificial solutions for manipulating, grasping, and transferring objects of different dimensions, weight, and textures with no damage in both agriculture and industrial applications.

Artificial suction cups can be classified based on their actuation method.[17] Passive suction cups mimic the natural structure of an octopus and exploit external preloads to adhere and attach to objects. They are effective at different scales, in both wet and dry environments.[2,4] On the other hand, active suction cups exploit soft actuators to create an inner negative pressure (Figure 1C). Fluidic actuation is the most used in suction cups[7,8,18–20] but there are also solutions that exploit shape memory alloys,[21,22] electrohydrodynamic pumps,[23] or dielectric electroactive polymers.[24,25]

Going beyond open-loop control entails integrating sensors into a soft body to provide sensory feedback. Ideally, to develop sensory suction cups (and soft robots), sensors should be: compliant to avoid negatively impacting on the mechanical properties of the body; sufficiently small to not hinder movement; resilient and robust to resist to mechanical stimulation; and repeatable.[26,27]

The sensing technologies used to replicate human touch capabilities range from resistive, capacitive, optical to magnetic and
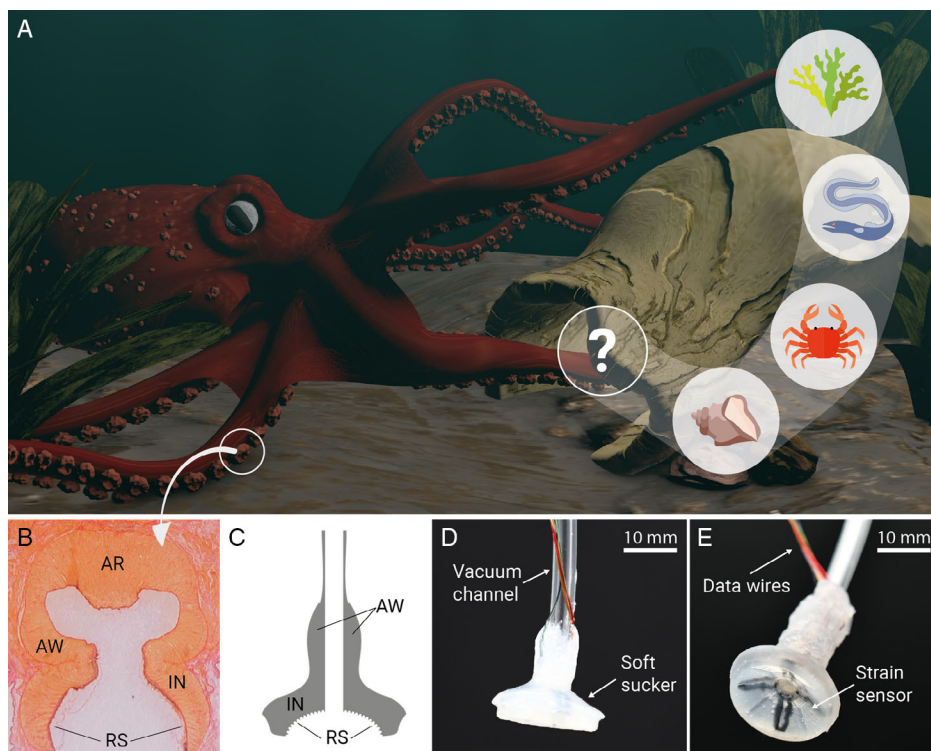
Figure 1. A) An overview of the "blind grasping" task. The octopus uses chemotactile receptors to locate, identify, and catch prey. With their suckers, octopuses can perceive tactile information and have a localized grasping capacity. B) A histological slice of the octopus suction cup taken from another study.[14] The sucker is composed of two main parts: the acetabulum (AR, acetabular roof, and AW, acetabular wall) and the infundibulum (IN). RS is a rough surface located on the infundibulum surface. C) Comparison of the artificial sucker. For the proposed artificial sucker to replicate the same morphology and function as a natural sucker, the following sections are included: the (AW) vacuum channel to create pressure changes within the suction cup, the (IN) artificial infundibulum wall that creates a sealed environment and provides tactile feedback, and the (RS) as a contact layer with the object. D, E) Artificial suckers. The sucker is made of soft materials that allow a passive adaptation to any object shape thereby improving suction (a vacuum pump is used to activate the sucker). The sucker also embeds four independent strain sensors that are used to acquire information on the stiffness of the touched object and the applied force.

barometric, and progress is also being made with force feedback sensors and texture recognition systems.[28–31] One popular approach is to create resistive-based sensors by embedding conductive fluids into the channels distributed in the soft bodies. When external forces or pressures are applied, a variation in resistance is obtained due to change in the channel geometry.[32–34] Capacitive sensors measure the changes in capacitance caused by changes in geometry due to the body deformation caused by an external force or pressure.[35–37] Optical strain sensors normally measure light intensity variation from a light source and a photoreceptor due to the deformation of the optical waveguide in between them.[38–40] Magnetic strain sensors embed a magnetic source and a magnetic field sensor into a soft body. As a result of an external load, this soft body deforms, causing a change of reading due to the change of the position and orientation of the sensor, with respect to the permanent magnet.[41] Barometric sensing can measure the pressure change in hydraulic or pneumatic circuits due to strain or compression for tactile sensing.[42]

To detect the proximity, contact, direction, imbalance, and weight of the object to grasp, sensory suction cups have been developed at varying scales and using different sensing

solutions[43–49] (Table S1, Supporting Information). Sareh et al.[43] developed an artificial sensorized sucker using fiber Bragg grating as a sensor which enables the sucker to understand whether it is in contact with an object. Huh et al.[44] integrated a set of pressure sensors into the suction cup to discern whether the contact is full or not. Lee et al.[45] used thin layers of carbon nanotubes as conductive materials to sensorize the artificial suction cup, enabling the detection of the relative position and imbalance of the object when grasped, as well as the estimation of the weight of the lifted body. Aoyagi et al. used PEDOT:PSS for adding sensing to an artificial suction cup, which can recognize the orientation of the object.[46] To enable the sucker to automatically identify its relative distance from the base plate to the surface of a suction cup, Doi et al. implemented a capacitive proximity sensor.[47]

All these studies highlight how sensorized suckers operate in harsh environments as grippers to recognize the objects. However, most of them only work in the air, and due to technological constraints, their sizes make them difficult to integrate into a soft arm. Moreover, none of them can identify the level of stiffness of an object, which is a feature of increasing interest in the scientific community for object detection[50–52] and medical applications.[31]

In this study, we developed a sensorized, active suction cup that morphologically resembles an octopus sucker. The sucker embeds four strain sensors, made up of microfluidic channels filled with conductive materials in a 90° configuration that allows the sucker to sense contact with objects (Figure 1D–E).

Based on extensive testing and validation, we proved that the proposed artificial suction cup can be used to classify a variety of materials with varying stiffness, both in air and in water. The suction cup can also identify the angle and direction of the contact using multilayer perceptron classification and regression, respectively. In addition, we evaluated the performance of different combinations of materials to cast the sucker, while keeping the whole system soft and adaptable to the surrounding environment. Our results show that the approach is consistent and repeatable, thus paving the way for the development of artificial suction cups with embedded and localized sensing capabilities for blind exploration and grasping applications.

2. Results and Discussion

2.1. Mechanical Characterization of the Artificial Suction Cup

The proposed artificial suction cup consists of two independent parts, which are merged to create a unique, soft structure (**Figure 2**A). To integrate sensing, we designed the top layer to host four microfluidic channels. These channels were filled with carbon grease (MG Chemicals) to act as four strain sensors embedded in the suction cup. The bottom layer is similar to the infundibulum of the natural sucker and its outer part has a series
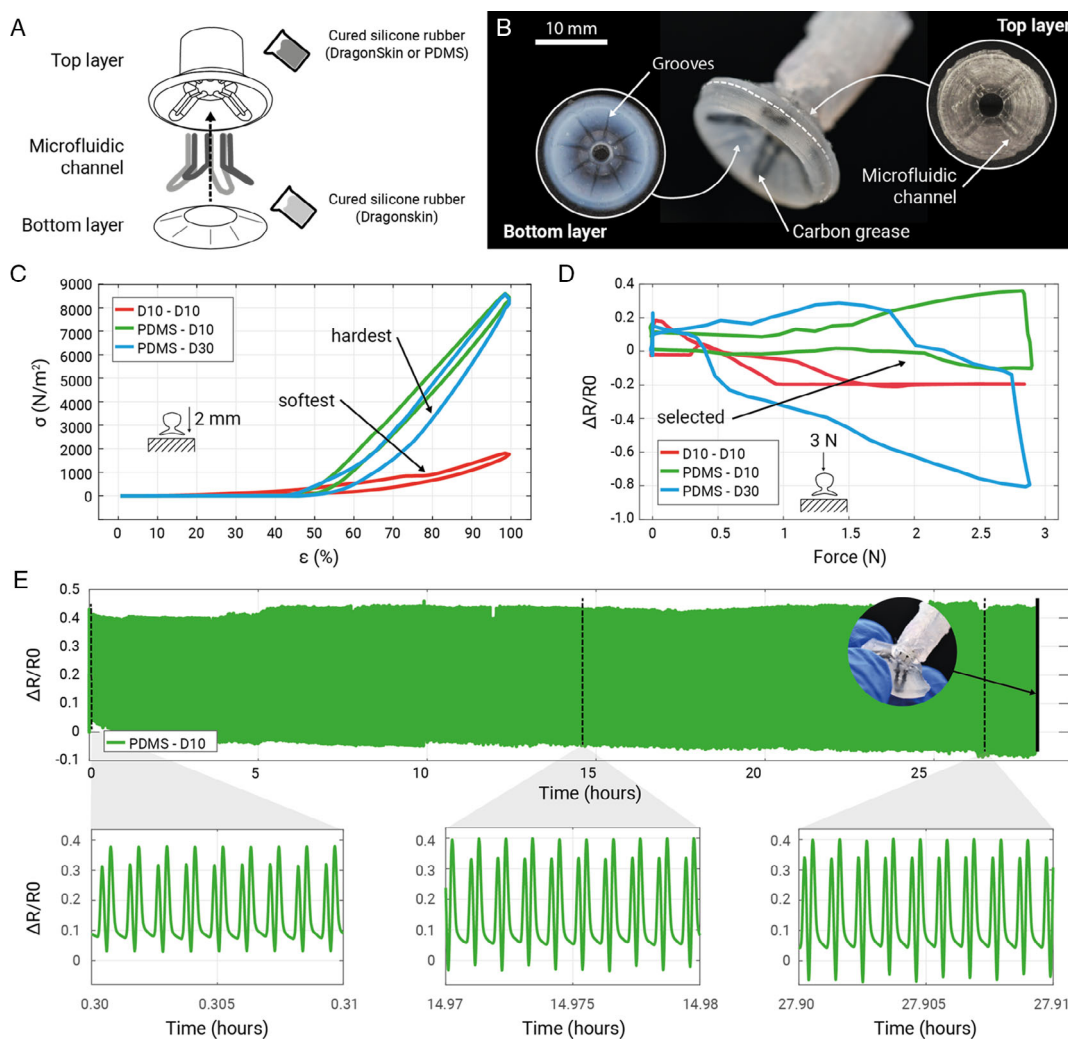

Figure 2. A) The artificial suction cup. It is made up of two parts: the top, which provides support for the vacuum channel and hosts the conductive material used for sensing; and the bottom, which is softer to ensure good adaptation and sensitivity with any substrate. B) Top and bottom parts when assembled into the soft artificial sucker. The bottom part also contains additional groves that allow for better grasping of the object. Both the top and lower parts have microfluidic channels that allow the material used to be injected for sensing purposes: carbon grease. C) Stress–strain characterization of three suckers with different combinations of materials for the top and bottom parts. D) Force-reading characterization of the embedded strain sensor considering the same sucker presented in (C). E) Repeatability evaluation of the sensor over 26 000 cycles with highlighted portions of the signal.

**ADVANCED
SCIENCE NEWS**
www.advancedsciencenews.com

**ADVANCED
INTELLIGENT
SYSTEMS**
Open Access

www.advintellsyst.com

of radial grooves which, like the biological counterpart, help in the passive adhesion to objects.[3] The suction cup has a diameter of 19 mm and is 10 mm in height. Each of the internal microfluidic channels has a cross-section of 600 μm, and the resulting sensor elements have a resistance in the range of 100–200 kΩ. A final version of the artificial sucker is presented in Figure 2B.

We first evaluated the performance of the proposed suction cup by varying the materials used in the casting of both the top and bottom parts (Figure S1 and S2, Supporting Information, show the complete manufacturing steps and the suction cup dimensions). The difference in the material composition means that different levels of sensitivity and compliance can be obtained when contacting an object. The purpose of this analysis is to find a good trade-off between the softness of the suction cup (which helps to achieve adaptability on different surfaces and therefore good sealing performance) and the dynamics of the sensor output (i.e., the ability to generate a signal variation for any deformation of the suction cup). We used a combination of Dragon Skin 10 (D10), Dragon Skin 20 (D20), Dragon Skin 30 (D30), and polydimethylsiloxane (PDMS). By combining the materials, we manufactured six suction cups (top-bottom): D10-D10, D20-D10, D30-D10, PDMS-D10, PDMS-D20, and PDMS-D30.

We applied a fixed displacement of 2 mm to each of these combinations and measured the reaction force when the suction cup was in contact with a hard substrate (Video S1, Supporting Information). When we used a soft material –such as D10– for both the top and lower parts, we obtained a highly adaptable sucker that can easily conform to any shape. However, the high compliance of the materials does not ensure a repeatable change in the cross section of the microchannel; thus, it is not possible to linearly map the resistance change in the strain sensors (Table S2, Supporting Information) because of the applied force/displacement. Instead, using hard materials—such as PDMS-D30—the sucker is rigid and less prone to deformations (Figure 2C contains three selected cases, the whole set is available in Figure S3, Supporting Information).

In order to correlate the sensor signal variation with the force exerted on the objects, we characterized the suction cups by evaluating their mean response to a force in the range of 0–3 N. When the suction cup is soft (D10–D10 combination), a small force (less than 1.5 N) is enough to achieve full suction cup deformation, and above that value the sensors do not work (red line in Figure 2D). On the other hand, a suction cup made of a combination of hard and soft materials (PDMS-D10) is less sensitive in a low force range but achieves a good level of sensitivity above 1 N (green line in Figure 2D). The stiffer one (PDMS-D30) provides wide signal variations, but their averaged readings were not suitable for mapping the $\Delta R \backslash R_0$ relationship (blue line in Figure 2D). Depending on the working range of the force required the most suitable materials can be selected.

Based on the results of the two validation tests, we selected the PDMS-D10 sucker because the combination of a "hard" sucker body (shore A50) and a "soft" interfacing layer (shore A10) enables an easy conformation of the sucker to any surface, while providing sufficient support for a repeatable change in the microchannel cross section, thus for a reliable change in the sensor readings. We tested the suction cup both in air and in water, actuating it at different vacuum pressure on several substrates with variable stiffness to evaluate the holding force. Results show

holding forces up to 8.7 N in air and 9.4 N in water (more details in Figure S4, Supporting Information).

To evaluate the suction cup durability, we further tested the selected sucker by acquiring the resistivity readings of the sensor in 26 000 cycle tests. In each test, the sucker was connected to a vertical slider which was set to move in the vertical direction with a fixed displacement of 2 mm performed at constant speed (Figure 2E). As in the previous experiment, we used a rigid plate as a substrate to ensure that all the displacement applied was transferred to the deformation of the sucker and not to the underlying structure. The results show that the sensorized sucker maintains its sensing capabilities with a variability of 0.05% over time (results of individual sensors are presented in Figure S5, Supporting Information). After 27 h of continuous testing, the suction cup cracked at the interface between the vacuum channel and the inner wall (inset Figure 2E). Nevertheless, the suction cup continued to function properly until the end of the experiment. A similar durability is expected in water, since it depends mostly on what the suction cup is made from. In fact, in this experiment, the artificial sucker is simply deformed without activating the suction. In contrast, in the case of suction, thanks to the better seal in water, the suction cup could be subjected to greater forces and therefore to higher stresses, causing a decrease in the working life.

2.2. Contact Positions and Angles Based on Embedded Sensors

In real environments, the suction cup can contact objects in any direction. If the rim of the suction cup does not adhere completely to the objects, the attachment cannot be achieved. Contact direction and angle help orient the suction cup toward the object so that it can be retrieved. Following the initial characterization tests, we evaluated the performance of the embedded sensors to detect independent contacts acting on each sensor and the relationship between the sensor readings and the contact angle. To better control and fix the experimental parameters, the suction cup was attached to a load cell (Nano17, ATI) connected to a linear stage (M-111 Compact Micro-Translation Stage, PI).

In an initial series of measurements, the slider moved the sucker vertically (2 mm) at constant velocity (0.5 mm s^{-1}) toward an object placed perpendicular to the motion direction. In each test, only one of the sensors actively touched the object. Video S2, Supporting Information, shows an example of the data acquired during the stimulation of each of the embedded sensors. This was possible by positioning the artificial sucker with a contact area of 25% above the object. We also acquired a set of measurements when the suction cup was in the air with no contact with any object. These are used to reference the signal and for a clearer understanding of the sensor readings. **Figure 3**A shows the sensor readings (means over 15 repeated measurements) plotted as a sequence of single events. In fact, it is possible to identify which sensor is active by simply using thresholding, but it is not possible to generalize a unique model to relate sensor readings to the applied force. In each test, we applied a fixed force profile, as shown in Figure 3B.

The graph highlights that a simple thresholding approach might be sufficient to identify which sensor is involved in the
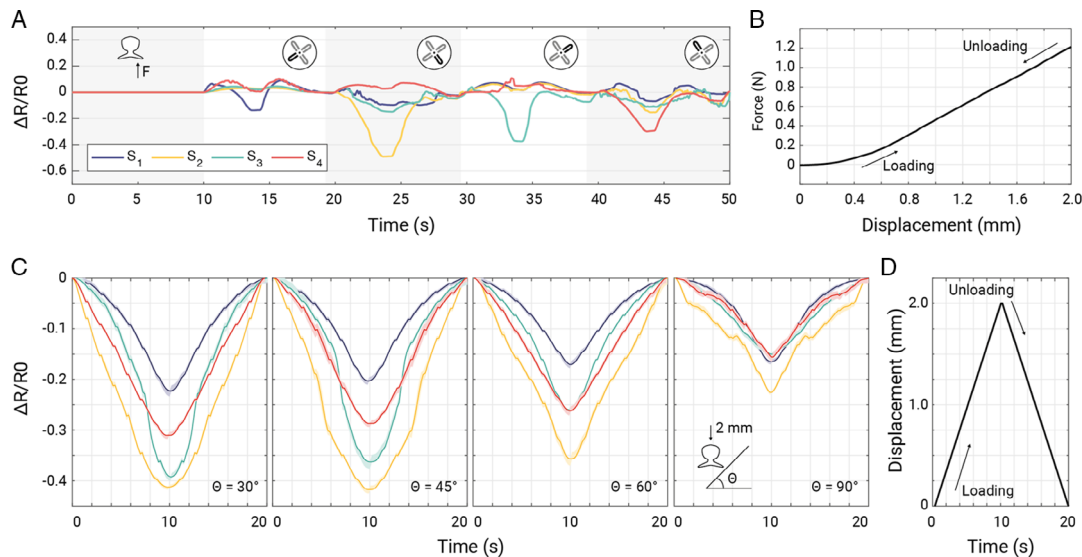
Figure 3. A) Variation of the signal upon a vertical displacement of 2 mm over a rigid surface. In each case, identified by the change in the background, only one sensor is touching the surface. Using simple thresholding, it is possible to identify which sensor is active, but it is not possible to generalize a unique model to relate the applied force to the sensor readings. B) Force profile followed during the measurements plotted in (A). C) Changes in the $\Delta R/R_0$ for each sensor when in contact with obstacles with different angles. For each case (30°, 45°, 60°, and 90°) only the readings of the sensor that was directly touching the object are plotted. As in (A), by considering the change in $\Delta R/R_0$, it is clear which sensor is active (all the other sensors have a lower $\Delta R/R_0$ compared to the active one). However, a unique model cannot be created that relates any type of sensor reading to a specific change in the object slope. D) Displacement profile of the measurements plotted in (C).

contact since its reading is the one that changes the most. However, due to the manufacturing, even if the same force profile is applied, the sensors respond in different ways, thus preventing a linear relationship between the sensor reading and the applied force. The different response of the sensors is due to a combination of factors: the manufacturing process, which requires several manual steps, can result in small differences in the realization of the sensor's channels; the carbon grease is not completely homogeneous and can have variable properties and its distribution in the channels may vary; and the perfect alignment of the suction cup with the target object is difficult to achieve and this can result in a different indentation between the four sensors.

Using the same experimental protocol, we replaced the object underneath the sensor with four different ones with angles of 30°, 45°, 60°, and 90° (Video S3, Supporting Information). We moved the sucker (2 mm) down at a constant speed (0.5 mm s^{-1}) and acquired the sensor readings (Figure 3C shows only the readings of the sensor that touched the object. The full dataset is presented in Figure S5, Supporting Information). We repeated the measurements 150 times for each sensor following the displacement profile plotted in Figure 3D. The experimental setup is shown in **Figure 4**A. As in the previous set of measurements, if we consider the maximum value of $\Delta R/R_0$, there is a clear change in the readings when the contact is considered as a single event, that is, when a contact happens under one of the sensors, its $\Delta R/R_0$ changes irrespectively of the angle. However, although in many cases there is a clear trend, due to inaccuracies in the fabrication of the sensors, it is not always possible to distinguish between the angle of the touched object and which sensor was involved in the contact.

2.3. Contact Position and Angles Based on Regression

As shown in Figure 3, the signal profiles of each sensor have a similar trend when referenced to their no-touch readings. In fact, there is a clear resistance variation at increasing angles for the touched sensor, while all the nontested sensors slightly change. However, the amount of the change and the response/recovery time differs for each sensor. Consequently, classical approaches such as simple thresholding are not possible. We thus applied machine learning to the raw sensor data to examine the relationship between the contact position and angle and the sensor readings. To do this, we implemented a neural network architecture that combines all the four sensor readings into a multidimensional input and then applied multilayer perception regression[50] in a supervised manner.

For the training of the network, we used the whole sequence of measurements of the four sensors acquired over time (i.e., during the downward and upward movement of the slider). The whole sequence means we can detect deformation on the suction cup for each sensor at a time. We trained a single-input, single-output model of a multilayer perceptron regression to predict the value of deformation for angles and contact directions and independent events. To predict the two values simultaneously, we used a single-input, multiple-output model of a multilayer perceptron regression. The algorithm applies layer normalization to every layer of the neural network. All neural network layers are activated by rectified linear units (ReLU), except the final layer which uses tanh to calculate the regression value. Both the models were trained, again using an 80–20 factor between training test sets (1920 samples) and validation test sets (480 samples), to reduce the chance of overfitting.
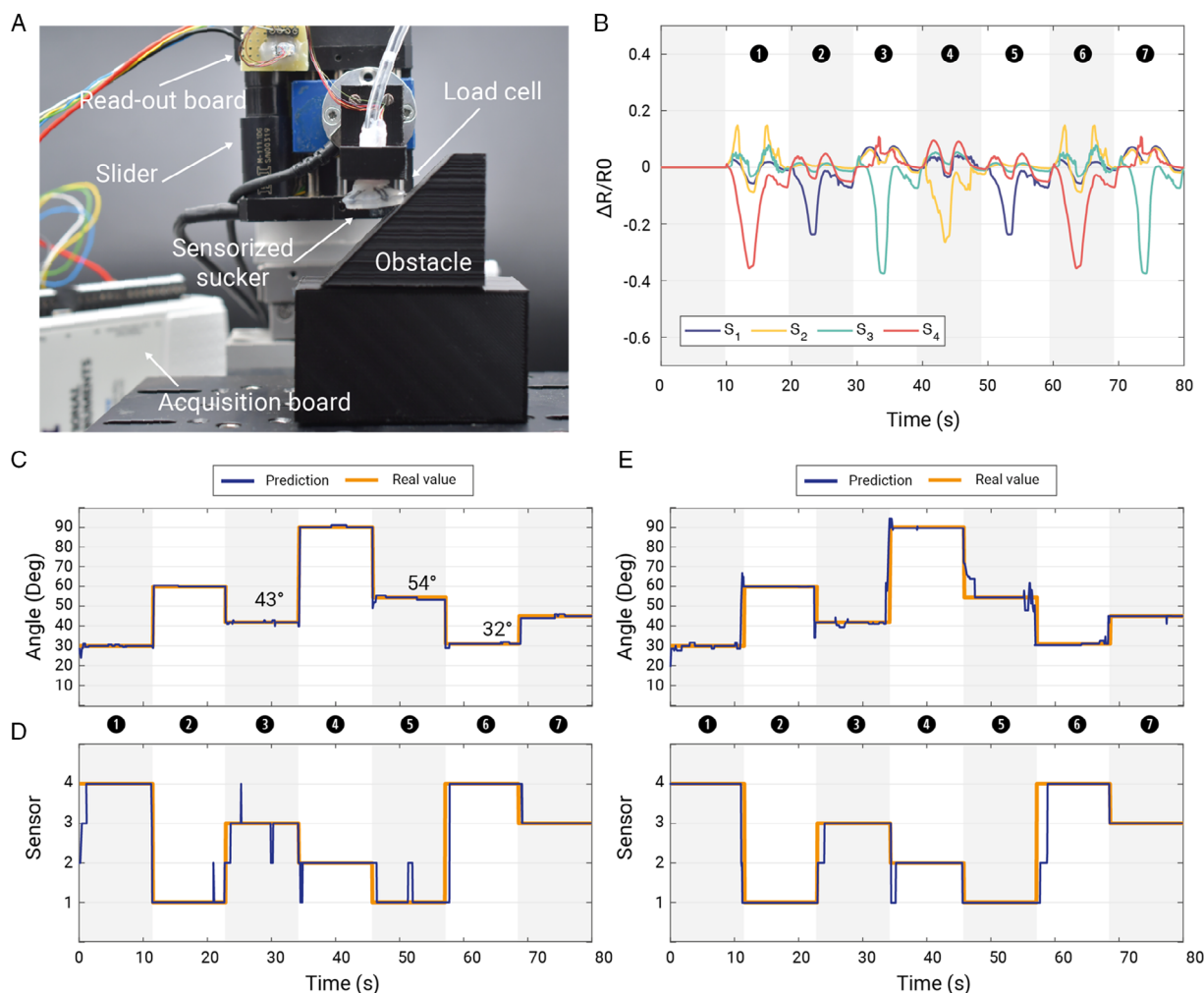
**ADVANCED
SCIENCE NEWS**

www.advancedsciencenews.com

**ADVANCED
INTELLIGENT
SYSTEMS**
Open Access

www.advintellsyst.com

Figure 4. A) Experimental setup used in both the characterization and evaluation phases. The sensorized suction cup is connected to a load cell attached to a slider that enables precise vertical movements. Each sensor is connected to the acquisition unit by a voltage divider. Data is collected in real time. B) Tested scenarios as a combination of single events with a direction and angle varying within the range of the trained samples (from 30° to 90°). 1) direction: 4, angle: 30°; 2) direction: 1, angle: 60°; 3) direction: 3, angle: 43°; 4) direction: 2, angle: 90°; 5) direction: 1, angle: 54°; 6) direction: 4, angle: 32°; 7) direction: 3, angle: 45°. C) Results of the regression using MLP considering a model that computes the contact angle only given the four sensor readings as an input, D) only the direction of contact, and E) simultaneously both the contact angle and the direction of contact given the four sensor readings as an input.

To evaluate the effectiveness of the approach, we considered a set of seven cases (Figure 4B) containing a combination of angle and direction like the one used in the training and validation phase (samples 1, 2, 4, 7) but also three new cases of angle values (samples 3, 5, 6 with values 43°, 54°, and 32° respectively). Figure 4C,D shows the results for the regression considering two independent models, one for the angle and one for the direction. A popular measure is the mean absolute error (MAE), which is defined as the number of errors versus the target value. Additionally, MAE changes are linear and therefore intuitive. The results with MAE values are 0.98 for angles, and 0.02 for directions.

We considered a merge of the two pieces of data into a single model that can predict, simultaneously, the direction and contact angle (Figure 4E). As in previous cases, using this model, the results show a rate of correctness of 2.72 MAE for the

simultaneous prediction of angle and direction. The results plotted in Figure 4C–E were obtained by considering blocks of signals with fixed dimensions (ten points) and they show the predictions of the expected final angle after a 2 mm displacement.

2.4. Material Characterization Based on Embedded Sensors

We tested the proposed sensory artificial sucker on samples with different shore hardness so that different materials could be classified. We selected a set of eight materials that ranged from 0010 to D50 shore hardness (Figure S6, Supporting Information). For each one, we manufactured $50 \times 50 \times 25$ mm³ blocks, which were first mechanically characterized to identify their stress–strain curves (Figure S7, Supporting Information) and then used to test the artificial sucker and its sensors. We first applied a vertical displacement of 2 mm on the sucker when in

contact with one of the selected materials, and we recorded the corresponding resistance variation. We repeated each test 15 times keeping the speed of the vertical displacement constant and holding in the sucker position for 1 s before moving it upward. **Figure 5**A shows the average signal for each of the sensors, and the standard deviation is below 0.02. Details on the experimental setup are presented in Figure S8, Supporting Information, while the computed standard deviation for each signal and material is summarized in Table S3, Supporting Information. The results suggest that with the increase in stiffness, the maximum resistance variation increases—consider the variation in the M-shaped signal—and all the sensors follow a similar trend. However, the range of change is not always linear with the increase in stiffness—consider the case of A50 vs. A80—and not uniform among the sensors.

Averaging the signal acquired from the sensors gives a clearer trend and a more regular change in the $\Delta R \backslash R_0$ (Figure 5B). We further subdivided the materials into four categories—soft, semisoft, semihard, and hard—to better identify common trends in the signal and thus to simplify their identification. From the results, the soft and semisoft materials show a change in the $\Delta R \backslash R_0$ that ranges from 0.05 to 0.4, with a mean variation of 0.2.

Although similar, due to their compliance, the soft materials produced a maximum change of 0.1 when the sucker was attaching/detaching itself from the material, while the semisoft ones reached a peak of 0.3. Similarly, semihard and hard materials shared the same change in $\Delta R \backslash R_0$, around 0.6; however, the measurements acquired during the "holding" stage varied. For semihard materials, the resistance variation reached up to 0, meaning that the material fills the inside wall of the sucker and pushes it to its original configuration; while in the hard materials this cannot happen and thus the sucker flattens on the surface limiting the change in resistance.

To assess the reliability of our sensing solution in different working environments, we repeated the same experiments both in the air and underwater. We compared the results considering the clustering in the four categories (Figure 5C,D) by averaging the signals of each group of materials (details on the standard
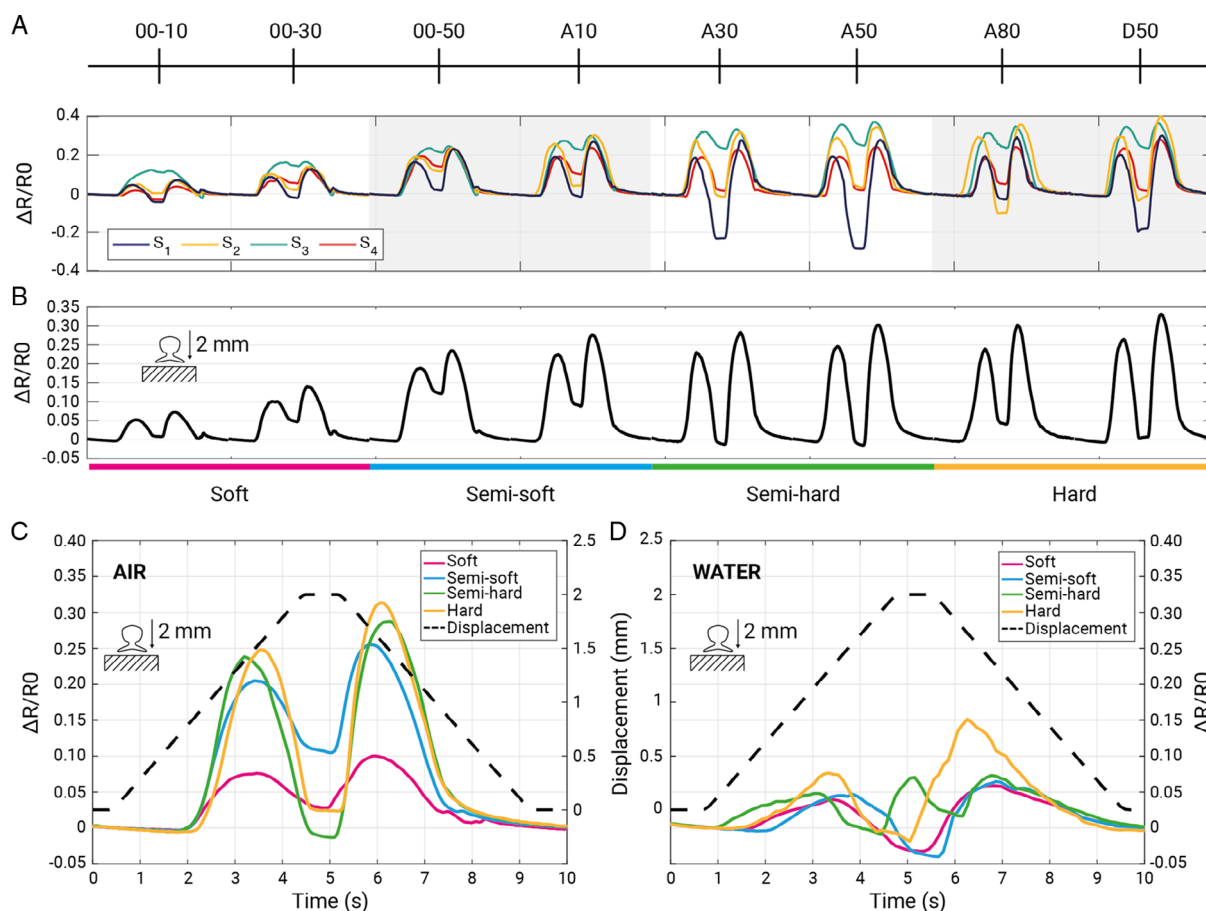

Figure 5. Material characterization based on the sensor readings. A) Individual strain sensor readings for each of the tested materials (from the softest, 0010 to the hardest, D50). The signal average is computed over 10 independent measurements. The changes in each strain sensor follow a similar trend, but they differ in the range of changes. B) Averaged strain sensor reading computed over the individual readings. Results are clustered according to larger categories—such as: soft, semisoft, semihard, and hard—based on the stiffness of the tested materials. This information reveals the same trend as in (A) together with a more defined and material-specific change in the measurement range. C) Comparison of the sensor readings for the four classes of materials. There is a clear, increasing change in the $\Delta R \backslash R_0$ as the materials become harder. D) Similar results are obtained when the sucker is tested in an underwater scenario. The main difference when compared to the tests in air (C) is $\Delta R \backslash R_0$ which decreases up to 0.4. Using machine learning, the trends in the signal change and its variation ($\Delta R \backslash R_0$) can be used to classify the different materials.

deviation are presented in Table S4 and S5, Supporting Information, for air and water, respectively). In air, the signal output from the embedded sensors has a regular behavior thanks to the direct interaction between the sucker, its sensor, and the material underneath. In water, instead, due to the change of medium, the readings and the trends change. The lower sensitivity of the suction cup in water is because the sensors become deformed to a lesser extent. This can be related to the water incompressibility (differently from air) and to the different friction on the substrates that result in a lower reaction force acting on the suction cup and consequently a reduced signal on the sensors (Figure S9, Supporting Information). Given that the results did not reveal a simple trend to enable a clear identification of the different materials, we used an approach based on machine learning to better identify any trends (Video S4 and S5, Supporting Information).

2.5. Material Classification Based on Machine Learning

The most common applications of machine learning are for solving classification problems requiring complex input signals, identifying features automatically from the data, and handling complex preprocessing workflows using well-known algorithms, such as k-nearest neighbor (KNN), feed-forward neural networks, or classical naive Bayesian methods. For more complex problems, such as object identification and recognition,[53] support vector machine (SVM) is one of the most effective supervised learning models,[54] while the multilayer perceptron is most effective when little is known about the structure of the problem.[55] In this application, we used multilayer perceptron as a standard algorithm to classify the materials both in air and in water. To assess performance, we repeated the vertical displacements test 120 times for each case (materials in air or water) keeping all the parameters constant.

First, we considered the air and water scenarios independently and trained the model by separating the data (**Figure 6**A). We kept the ratio constant between the training and the validation set by fixing it to 80–20 of the data as in the previous analysis. A total of 195 data values of individually recorded signals were considered for each contact with an object. The preprocessing of the data was filtered with a moving average (window size 10 samples). In all the cases, 195 data points are considered as the input to the network which outputs the body stiffness. We trained the model and computed the confusion matrices first considering the two scenarios separately with four classes each (Figure 6B and S11, Supporting Information, for the confusion matrix of the training and test sets, respectively). We then used the whole dataset to create a unique model that merged all the eight possible classes (Figure 6C and S12, Supporting Information, for the confusion matrix of the training and test sets, respectively).

The results show that the use of one single model improves the overall accuracy in the classification reducing the errors only in a few cases related to the underwater scenarios. In addition, considering the future integration of the model in an embedded
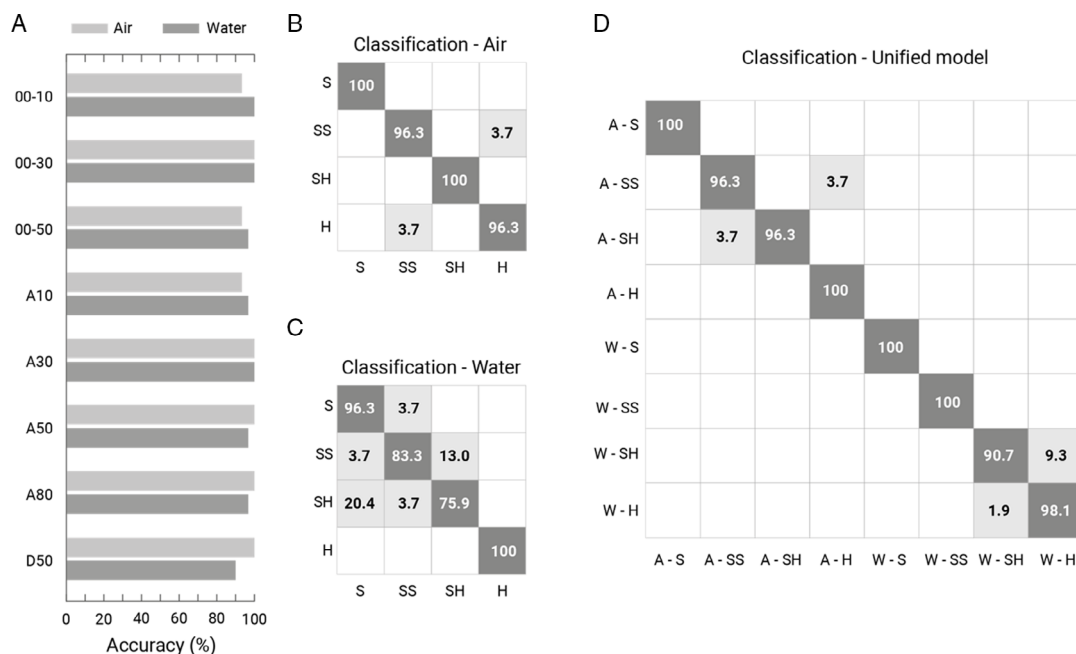

Figure 6. A) Comparison of the accuracy of the multilayer perceptron for the classification of the material in air or in water. Both the cases have comparable, promising results (>93%) with classification in air having a slightly better performance with 97.5% of accuracy in mean over the 97.1% in water. B) Confusion matrices, considering two independent models to classify the materials when the contact happens in air or in water. It is not surprising that the water classification model has more errors than the air classification model. This could be related to the presence of bubbles trapped between the artificial infundibulum and the object surface, which acts as an additional and variable interface between the material and the sensorized suction cup that affects the sensors readings (Figure S10, Supporting Information). C) Confusion matrix when a single model is used to classify both cases in air and water. By increasing the number of trained data, the overall performance improves slightly and in addition, it simplifies the model deployment in future applications.

decision system, a single model simplifies the deployment and the execution time when implemented in an ML-enabled microcontroller.

3. Conclusions

We have developed a soft artificial suction cup with integrated tactile sensing for detecting the angles, direction, and stiffness of differently shaped objects (Figure 1). While angle and direction are useful for orienting the suction cup toward the object to be grasped, the stiffness works particularly well for tissue palpation in medicine[31] and for ripeness assessment in precision agriculture.[56,57] Our solution is scalable (suction cup diameter 19 mm), thus enabling future integration in a soft octopus-like robotic arm. We studied how the design and the choice of the materials used to manufacture the artificial sucker affect its mechanical properties and sensing capabilities (Figure 2).

After selecting the final combination, we tested the sensorized suction cup in a wide range of stiffnesses (range from 0010 to D50) of different objects (Figure S6, Supporting Information). When the sensors are configured at a 90° angle to each other, it is also possible to detect the direction of contact with the object as well as the angle of contact. This was made possible by applying a machine learning (ML) approach to the acquired data. In fact, our initial analysis showed that the interaction between the artificial sucker and the different materials did not generate a clear trend in the sensor data (Figure 5). Thus, it was not possible to use a simple threshold cue-based classification to discriminate between the different materials. In addition, the test performed in water provided different trends in the sensors with respect to the test in air. This was due to a reduced sensibility of the suction cup in water caused by a lower reaction force. For this reason, the use of ML was considered.

We evaluated the accuracy of the method by acquiring 120 samples for each configuration (i.e., single material in air/water) and then selected the best one for the application. Two independent models were first trained to identify the materials both when the contact is in air or in water.

The models predicted the class of the material touched in the air with a 97.9% accuracy and underwater with a 93.5% accuracy. By combining the two pieces of information, we created a third model that categorizes all possible cases where we detect air and water simultaneously. Again, the results were promising with 95.8% accuracy (Figure 6A–C). Unlike the application that detected the stiffness of material, it was not possible to identify a single, reliable model that comprises all the features. We thus used regression to identify the contact position or angle that can find the specific value for the contact position or angle. Our results showed a correctness of 0.98, 0.02, and 2.72 for the MAE value for angles, directions, and both angles and directions at the same time; see Figure 4C–E.

Although our results are promising even though they derive from a simplified case (flat objects and suction cup indentation perpendicular to that surface). Identifying real objects in life will require further development in sensing technology and a longer training process. However, we believe that our solution opens the path for the development of novel technologies based on suction cups to be used for complex manipulation. The absence of rigid

parts and the scalability of the manufacturing process make the proposed suction cup a possible candidate for future integration in artificial arms inspired by octopuses that can locate and manipulate complex objects in environments where other senses are not available.

4. Experimental Section

Design and Fabrication of the Artificial Suction Cup: Designs for the sucker and required molds were created using 3D CAD (Solid Works 2019, Dassault Systems SolidWorks Corp, USA). The suction cup was composed of a top part with embedded microfluidic channels (the diameter of the channels was 600 μm) and the bottom part with the eight grooves (Figure 2B). A polylactic acid (PLA) filament was used to print the molds (Prusa MK3S+, filament diameter 1.75 mm, nozzle diameter 0.4 mm). During the first step of the casting, a fixed amount (4 mL) of PDMS (Sylgard 184) was poured into the mold, followed by 10 min degassing of the silicone rubber in a vacuum chamber. An internal mask was then laser cut from a Kapton sheet (50 μm) and placed on the sucker's surface after curing to aid in the placement of the sensors. Eight electric wires were placed to contact the microfluidic channels that were filled with carbon conductive grease (MG Chemicals, 846–80 G) and then the lower part of the suction was molded (Figure 2B). The second part of the casting was done to encapsulate the carbon conductive grease avoiding contact with environment.

Design and Fabrication of the Material Samples: The material samples were fabricated in blocks of 50 × 50 × 25 mm with the following techniques and materials (Figure S6, Supporting Information) (**Table 1**).

Characterization of the Suckers and Material Samples: Vertical indentation tests on the materials and on the artificial sucker were performed using a linear stage (M-111 Compact Micro-Translation Stage, PI). A 6-DOF load cell (Nano17, ATI), with the $+X$ axis pointing upward, was fixed to the slider and used to acquire the measurements. In the material characterization case, a rigid square probe (3 × 3 cm) was connected to the load cell and the slider moved at constant speed (0.5 mm s^{-1}) for 2 mm. In the artificial sucker case, instead, the sucker was fixed to a holder connected to the load cell and it moved toward a rigid plane at the same speed and for the same displacement as in the previous case. Before each measurement, the readings of the load cell were offset to provide a common reference. For all the experiments, the measurements were repeated at least 15 times.

Sensor Data Acquisition and Processing: The four resistive strain sensors on the artificial suction cup were connected to a dedicated voltage divider with a fixed resistor (ranging from 100–200 kΩ). Data was then sampled at 100 Hz by a data acquisition board (USB-6218, National Instruments, USA) and stored on a computer. Prior to further processing, raw data was filtered with a moving average (window size ten samples). Measurements recorded in air and underwater for each object and stored in CSV format. Acquired data was processed using MATLAB (MATLAB 2021a, MathWorks Inc.).

Table 1. Shore hardness and manufacturing process.

Shore hardness	Fabrication technique	Material
0010	Casting	Ecoflex 00-10, Smooth-On Inc.
0030	Casting	Ecoflex 00-30, Smooth-On Inc.
0050	Casting	Ecoflex 00-50, Smooth-On Inc.
A-10	Casting	Dragon Skin 10, Smooth-On Inc.
A-30	Casting	Dragon Skin 30, Smooth-On Inc.
A-50	SLA printing	Elastic 50 A Resin, Formlabs
A-80	SLA printing	Flexible 80 A Resin, Formlabs
D-50	FFF printing	PLA, Prusa Research a.s.

Machine Learning: The multilayer perceptron neural network consists of an input layer with a size equal to the feature vector, two hidden layers that have ten and six neurons, and an output layer containing one neuron per result considered. Each layer of the neural network uses ReLUs, except for the final layer, which uses tanh for regression or softmax for classification. To train categorical classifiers, 120 sample tests, which each included 195 points, were collected during data acquisition and processing of the selected suction cup, while 2400 sample tests that included 232 points were used for training the regression.

Repeatability and Durability Tests: The artificial suction cup was tested for repeatability and durability using the measurement setup shown in Figure S8, Supporting Information. The suction cup was attached to a six-axis torque sensor (Nano 17, ATI) connected to a linear stage (*M*-111 Compact Micro-Translation Stage, PI). In the repeatability tests, the linear stage was programmed to go up and down (with a stroke of 2 mm and a speed of 0.5 mm s^{-1}) until suction cup breakage, which provides information not only on the repeatability but also on the durability of the suction cup.

Supporting Information

Supporting Information is available from the Wiley Online Library or from the author.

Acknowledgements

Conflict of Interest

The authors declare no conflict of interest.

Data Availability Statement

The data that support the findings of this study are available on request from the corresponding author. The data are not publicly available due to privacy or ethical restrictions.

Keywords

[1] C. Laschi, B. Mazzolai, M. Cianchetti, *Sci. Robot.* **2016**, *1*, eaah3690.
[2] F. Tramacere, L. Beccai, F. Mattioli, E. Sinibaldi, B. Mazzolai, IEEE, Piscataway, NJ **2012**, pp. 3846–3851.
[3] F. Tramacere, M. Follador, N. Pugno, B. Mazzolai, *Bioinspir. Biomimet.* **2015**, *10*, 035004.
[4] S. Baik, Y. Park, T.-J. Lee, S. H. Bhang, C. Pang, *Nature* **2017**, *546*, 396.
[5] I. D. Walker, D. M. Dawson, T. Flash, F. W. Grasso, R. T. Hanlon, B. Hochner, W. M. Kier, C. C. Pagano, C. D. Rahn, Q. M. Zhang, in *Unmanned Ground Vehicle Technology VII* International Society For Optics And Photonics, Bellingham, WA **2005**, pp. 303–314.
[6] C. Laschi, M. Cianchetti, B. Mazzolai, L. Margheri, M. Follador, P. Dario, *Adv. Robot.* **2012**, *26*, 709.
[7] Z. Xie, A. G. Domel, N. An, C. Green, Z. Gong, T. Wang, E. M. Knubben, J. C. Weaver, K. Bertoldi, L. Wen, *Soft Robot.* **2020**, *7*, 639.
[8] B. Mazzolai, A. Mondini, F. Tramacere, G. Riccomi, A. Sadeghi, G. Giordano, E. Del Dottore, M. Scaccia, M. Zampato, S. Carminati, *Adv. Intell. Syst.* **2019**, *1*, 1900041.
[9] W. M. Kier, A. M. Smith, *Integr. Comparat. Biol.* **2002**, *42*, 1146.
[10] G. Sumbre, G. Fiorito, T. Flash, B. Hochner, *Curr. Biol.* **2006**, *16*, 767.
[11] J. A. Mather, *J. Comparat. Psychol.* **1998**, *112*, 306.
[12] P. Graziadei, *Nature* **1962**, *195*, 57.
[13] P. Graziadei, H. Gagne, *Tissue Cell* **1976**, *8*, 229.
[14] F. Tramacere, L. Beccai, M. Kuba, A. Gozzi, A. Bifone, B. Mazzolai, *PLoS One* **2013**, *8*, 65074.
[15] M. J. Wells, *Octopus: Physiology And Behaviour Of An Advanced Invertebrate*, Springer Science & Business Media, New York **2013**.
[16] M. J. Wells, *Q. J. Exp. Psychol.* **1964**, *16*, 156.
[17] H. Bagheri, S. Berman, M. M. Peet, D. M. Aukes, X. He, S. C. Pratt, R. E. Fisher, H. Marvi, *Bioinspired Sensing, Actuation, And Control In Underwater Soft Robotic Systems*, Springer, New York **2021**, pp. 189–212.
[18] T. Tomokazu, S. Kikuchi, M. Suzuki, S. Aoyagi, in *IEEE/RSJ International Conference on Intelligent Robots and Systems (IROS)*, IEEE, Piscataway, NJ **2015**, pp. 2929–2936.
[19] Y. Tang, Q. Zhang, G. Lin, J. Yin, *Soft Robot.* **2018**, *5*, 592.
[20] A. Koivikko, D.-M. Drotlef, C. B. Dayan, V. Sariola, M. Sitti, *Adv. Intell. Syst.* **2021**, *3*, 2100034.
[21] H. Bing-Shan, W. Li-Wen, F. Zhuang, Z. Yan-zheng, *Int. J. Adv. Robot. Syst.* **2009**, *6*, 29.
[22] B. Hu, Z. Dong, Z. Fu, Y. Zhao, in *Earth & Space 2008: Engineering, Science, Construction, And Operations In Challenging Environments*, **2008**, pp. 1–8. 10.1061/40988(323)187
[23] Y. Kuwajima, H. Shigemune, V. Cacucciolo, M. Cianchetti, C. Laschi, S. Maeda, IEEE, Piscataway, NJ **2017**, pp. 470–475.
[24] M. Follador, F. Tramacere, B. Mazzolai, *Bioinspir. Biomimet.* **2014**, *9*, 046002.
[25] N. Sholl, A. Moss, W. M. Kier, K. Mohseni, *Soft Robot.* **2019**, *6*, 356.
[26] H. Wang, M. Totaro, L. Beccai, *Adv. Sci.* **2018**, *5*, 1800541.
[27] P. Roberts, M. Zadan, C. Majidi, *Curr. Robot. Rep.* **2021**, *2*, 343.
[28] Y. Xin, M. Cui, C. Liu, T. Hou, L. Liu, C. Qian, Y. Yan, *Rev. Sci. Instrum.* **2021**, *92*, 095003.
[29] Y. Liu, S. Cui, J. Wei, H. Li, J. Hu, S. Chen, Y. Chen, Y. Ma, S. Wang, X. Feng, *Adv. Intell. Syst.* **2022**, *4*, 2100072.
[30] Y. Li, M. Zhao, Y. Yan, L. He, Y. Wang, Z. Xiong, S. Wang, Y. Bai, F. Sun, Q. Lu, *NPJ Flex. Electron.* **2022**, *6*, 1.
[31] J. Huang, A. Rosendo, *Soft Robot.* **2022**, *1*. https://doi.org/10.1089/soro.2021.0105.
[32] J. Shintake, Y. Piskarev, S. H. Jeong, D. Floreano, *Adv. Mater. Technol.* **2018**, *3*, 1700284.
[33] C. Ren, X. Ding, W. Li, H. Wu, H. Yang, *J. Chem. Eng. Data* **2017**, *62*, 1865.
[34] S. Xu, D. M. Vogt, W.-H. Hsu, J. Osborne, T. Walsh, J. R. Foster, S. K. Sullivan, V. C. Smith, A. W. Rousing, E. C. Goldfield, R. J. Wood, *Adv. Funct. Mater.* **2019**, *29*, 1807058.
[35] L. Viry, A. Levi, M. Totaro, A. Mondini, V. Mattoli, B. Mazzolai, L. Beccai, *Adv. Mater.* **2014**, *26*, 2659.
[36] A. Atalay, V. Sanchez, O. Atalay, D. M. Vogt, F. Haufe, R. J. Wood, C. J. Walsh, *Adv. Mater. Technol.* **2017**, *2*, 1700136.
[37] O. Atalay, A. Atalay, J. Gafford, C. Walsh, *Adv. Mater. Technol.* **2018**, *3*, 1700237.

[38] S. Sareh, Y. Noh, M. Li, T. Ranzani, H. Liu, K. Althoefer, *Smart Mater. Struct.* **2015**, *24*, 125024.

[39] H. Zhao, K. O'Brien, S. Li, R. F. Shepherd, *Sci. Robot.* **2016**, *1*, eaai7529.

[40] Y. Du, Q. Yang, J. Huang, *IEEE Sens. J.* **2017**, *17*, 7455.

[41] M. Luo, E. H. Skorina, W. Tao, F. Chen, S. Ozel, Y. Sun, C. D. Onal, *Soft Robot.* **2017**, *4*, 117.

[42] D. Gong, R. He, J. Yu, G. Zuo, *Sensors* **2017**, *17*, 2592.

[43] S. Sareh, K. Althoefer, M. Li, Y. Noh, F. Tramacere, P. Sareh, B. Mazzolai, M. Kovac, *J. Roy. Soc. Interface* **2017**, *14*, 20170395.

[44] T. M. Huh, K. Sanders, M. Danielczuk, M. Li, Y. Chen, K. Goldberg, H. S. Stuart, in *IEEE/RSJ Int. Conf. on Intelligent Robots and Systems (IROS)*, IEEE, Piscataway, NJ **2021**, pp. 1786–1793.

[45] H. J. Lee, S. Baik, G. W. Hwang, J. H. Song, D. W. Kim, B. Park, H. Min, J. K. Kim, J. Koh, T.-H. Yang, *ACS Nano* **2021**, *15*, 14137.

[46] S. Aoyagi, M. Suzuki, T. Morita, T. Takahashi, H. Takise, *IEEE/ASME Trans. Mechatron.* **2020**, *25*, 2501.

[47] S. Doi, H. Koga, T. Seki, Y. Okuno, in *2020 IEEE Int. Conf. Rob. Autom. (ICRA)*, IEEE, Piscataway, NJ **2020**, pp. 638–643.

[48] S. T. Frey, A. B. M. T. Haque, R. Tutika, E. V. Krotz, C. Lee, C. B. Haverkamp, E. J. Markvicka, M. D. Bartlett, *Sci. Adv.* **2022**, *8*, eabq1905.

[49] S. Zhuo, Z. Zhao, Z. Xie, Y. Hao, Y. Xu, T. Zhao, H. Li, E. M. Knubben, L. Wen, L. Jiang, M. Liu, *Sci. Adv.* **2020**, *6*, eaax1464.

[50] J. Hughes, A. Spielberg, M. Chounlakone, G. Chang, W. Matusik, D. Rus, *Adv. Intell. Syst.* **2020**, *2*, 2000002.

[51] M. Bednarek, P. Kicki, J. Bednarek, K. Walas, *Electronics* **2021**, *10*, 96.

[52] Y. Yan, C. Cheng, M. Guan, J. Zhang, Y. Wang, *Machines* **2022**, *10*, 173.

[53] G. Zhao, J. Yang, J. Chen, G. Zhu, Z. Jiang, X. Liu, G. Niu, Z. L. Wang, B. Zhang, *Adv. Mater. Technol.* **2019**, *4*, 1800167.

[54] S. Shin, H. U. Yoon, B. Yoo, *Sensors* **2021**, *21*, 3204.

[55] U. Orhan, M. Hekim, M. Ozer, *Expert Syst. Appl.* **2011**, *38*, 13475.

[56] C. T. Christopher, A. M. R. Fath Elbab, C. O. Osueke, B. W. Ikua, D. N. Sila, A. Fouly, *Cogent Eng.* **2022**, *9*, 2030098.

[57] F. E. Erukainure, V. Parque, M. A. Hassan, A. M. R. FathElbab, in *IEEE/ASME Int. Conf. on Advanced Intelligent Mechatronics (AIM)*, IEEE, Piscataway, NJ **2022**, pp. 290–295.